Queen's University
Belfast

Optical Thomson scatter from a laser-ablated magnesium plume

Published in:
Journal of Applied Physics

Document Version:
Publisher's PDF, also known as Version of record

Queen's University Belfast - Research Portal:
Link to publication record in Queen's University Belfast Research Portal

Optical Thomson scatter from a laser-ablated magnesium plume

A. Delserieys, F. Y. Khattak,[a)] C. L. S. Lewis, and D. Riley[b)]

School of Mathematics and Physics, Queen's University Belfast, Belfast BT7 1NN, United Kingdom

We have carried out an optical Thomson scatter study of a KrF laser-ablated Mg plume. The evolution of the electron temperature and density at distances 2–5 mm from the target surface has been studied. We have observed that the electron density falls more rapidly than the atomic density and believe that this is a result of rapid dielectronic recombination. A comparison of the electron density profile and evolution with simple hydrodynamic modeling indicates that there is a strong absorption of the laser in the plasma vapor above the target, probably due to photoionization. We also conclude that an isothermal model of expansion better fits the data than an isentropic expansion model. Finally, we compared data obtained from Thomson scatter with those obtained by emission spectroscopy under similar conditions. The two sets of data have differences but are broadly consistent. © 2009 American Institute of Physics. [doi:10.1063/1.3251366]

I. INTRODUCTION

There is a great deal of interest in laser-ablated plumes at temperatures of ~1 eV due to their significant technological potential.[1–7] For example, in pulsed laser deposition (PLD) of thin films, the technique has the advantages of preserving the stoichiometry of the target material, having an energy source located outside the vacuum vessel and being capable of rapid growth rates. The plume conditions are of great interest to scientists developing the techniques and have been investigated with a variety of diagnostics.[8–13] Recently we have implemented spectrally resolved optical Thomson scatter from such plasmas.[14] This is a powerful diagnostic tool[15–18] that has been applied to a variety of plasmas including tokamaks,[19,20] high temperature laser plasmas,[21] as well as rf discharge plasmas and arc discharges.[22–24] However, only very little work has been done on this diagnostic technique for laser ablation plumes of the sort that are interesting for PLD work, for example, Ref. 25. In this paper, we present a study of Thomson scatter from laser-ablated plumes that expands on the preliminary paper published earlier.[14]

II. EXPERIMENTAL

Figure 1 shows a schematic of our experiment. The plasma is created with a KrF laser (Lambda Physik LPX 210*i*) of 20 ns [full width at half maximum (FWHM)] duration at 248 nm. Random phase plates[26] are used with a pair of cylindrical lenses to create a 1 mm^2 spot resulting in ~9 J/cm^2 onto a rotating Mg block (the intensity on target was thus ~0.5 GW cm^{-2}). At a controlled delay time, a frequency doubled Nd:YAG (yttrium aluminum garnet) pulsed laser (9 ns, 400 mJ at 532 nm) is used to probe a slice of the plume at a predetermined distance from the target surface at delays ranging from 100 ns to 1 μs.

The probe is loosely focused (f/200) with a focal spot diameter ~0.5 mm FWHM. The scattered radiation at 90° was collected by a lens and relayed to the imaging double grating spectrometer (SPEX 750 spectrometer, 1200 l/mm, dispersion 5.7 Å/mm) which was fitted with an Andor intensified charge-coupled device (ICCD) camera with a 10 ns gate, synchronized to collect the scatter signal and thus allowing a great reduction in plasma self-emission recorded. The image of the plasma plume was focused onto the spectrometer slit so that the lateral expansion direction, parallel to the target surface, was imaged along the slit length so as to give spatial resolution in that direction. The imaging was 1:1 from the slit to the CCD input. The spatial resolution along the axial direction is provided by moving the relative position of the 2ω probe beam and target. The spatial resolution in the axial direction was given by the slit width, which was 100 μm.

Great care was taken to equip the chamber with opaque materials and apparatus to reduce the stray light; part of it is represented in Fig. 1. The scattering signal was averaged over a minimum of 500 shots with the lasers running at 10 Hz, giving a good reproducibility. The detection system was calibrated by filling the chamber with 4 mbars of Ar gas. The known Rayleigh scatter cross section for this gas[27] could
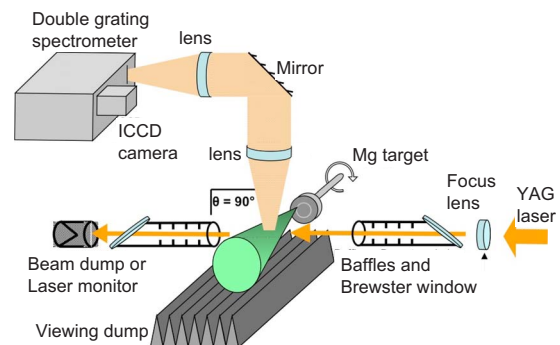

FIG. 1. (Color online) Schematic of setup for Thomson scatter. The baffle arms are fitted with Brewster angle windows to reduce stray light scatter, a double grating spectrometer with a gated (10 ns) ICCD camera is used.

[a)]Present address: Department of Physics, Kohat University of Science and Technology, Kohat-26000, NWFP, Pakistan.
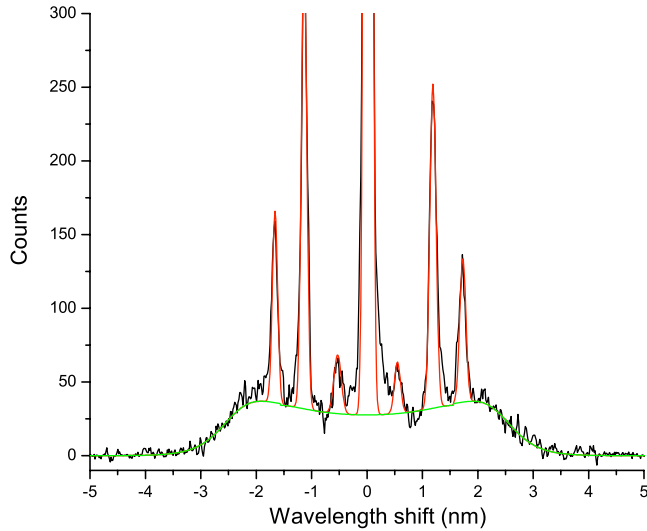[b)]Electronic mail: d.riley@qub.ac.uk.

FIG. 2. (Color online) Sample spectrum taken at a delay of 300 ns and 2 mm from the target surface. The fit curve shows a moderate α of 1.3 in the collective scatter regime. Also shown is the fitting to the Raman satellites which were subtracted in the fitting of the Thomson scatter.

then be used to compare the scatter signal and the measured energy of the laser pulse. In this way, we were able to infer the electron density, at the lower densities, from the overall Thomson scatter and the temperature from the shape of the scatter spectrum, assuming a Maxwellian electron distribution.

Figure 2 shows an example spectrum (see Ref. 14 for other examples). The central Rayleigh scatter from bound electrons is clearly seen. There are some interesting satellite features present with three peaks at separations of $\sim$20, $\sim$40, $\sim$60 cm^{-1} on each side of the Rayleigh peak. The spacings are consistent with atomic Raman transitions from the $^3P^0$ metastable states of Mg I.[28] A separate paper deals with these satellites.[29] The shape of the scattered spectrum is governed by the scattering parameter $\alpha = \lambda_0/4\pi\sin(\theta/2)\lambda_D$ where λ_0 is the probing wavelength, θ is the scattering angle and λ_D is the Debye length. If $\alpha \gtrsim 1$, then we probe collective oscillations of the electrons; for $\alpha \ll 1$ we probe the random thermal motion. To determine the electron temperature T_e and the electron density n_e from the scattering signal, two methods were used, depending on the shape of the spectrum. At lower α cases, we used a Gaussian fit to temperature and the overall level of scatter signal to determine density. For higher α cases, where there are clear plasmons as in Fig. 2, the fitting to density and temperature was done using the Salpeter approximation.[15] The fit is clearly seen in the figure, where we have $T_e = 1.2 \pm 0.3$ eV and $n_e = (2.6 \pm 0.8) \times 10^{16}$ cm^{-3}. Care was taken to account for the Raman satellites by fitting them to a Gaussian to be subtracted from the signal. The scattering parameter is $\alpha \sim 1.3$. An important issue is the possible perturbation of the plasma by the probe. In the higher density cases, e.g., at $t = 200$ ns, 2 mm from the target, the experiment was repeated with lower laser energies and more shots. A rise of T_e of $\sim$0.3 eV was measured, for the highest energy (200 mJ) compared to using only 50 mJ and the data are presented for the latter case where we esti-

mate that the effect is marginal ($\delta T < 0.1$ eV). As the plasma expands to lower density, the heating rapidly becomes much weaker, with even less perturbation.

III. RESULTS AND DISCUSSION

A. Axial expansion data

Figure 3 shows the time evolution of electron density and temperature along the axis of the expanding plume taken at four distances from the target surface. The densities are broadly consistent with previous interferometry and laser induced fluorescence measurements.[13,30] We can see evidence of a rise and subsequent fall in density as the plasma plume takes time to arrive at a particular point in space, with velocity $\sim 10^6$ cm s^{-1}. We have fitted power laws to the subsequent decay of the electron density with time and find that the density falls off more rapidly than the $n_e \propto t^{-3}$ expected from a simple three-dimensional (3D) adiabatic expansion of an initially thin, uniform 1 mm^2 slab of plasma.[31]

The intensity of the Rayleigh scattering signal, which is proportional to the density of atoms, does, however, follow this density scaling power law. We can see this in Fig. 4(a) where we have plotted the normalized Rayleigh signal and Thomson scatter signals. We fitted a power law of the form at^{-3} to the density of atoms (given by the Rayleigh peak intensity) and a fit of the form $bt^{-3}e^{-t/t_0}$ to the electron density. Here a and b are constants and t_0 plays the role of a typical time scale for reduction in the average ionization. Experimentally, we estimate this to be $\sim$230 ns. There are two possible ways in which the ionization can be seen to drop, both of which may occur. First, the plasma reaching the measurement point later in time originates from deeper inside of the target surface. It is therefore possible that, due to nonuniformity of the initially heated slab, it has a lower level of ionization to begin with and this is reflected in the lower electron density measured at a fixed point later in time. Another option is that recombination of the electrons with the ions is occurring. In order to tell if recombination is occurring, we can follow a fluid element of the plasma in time along the axial expansion. We can do this, if we have an estimate of the expansion velocity and measurements at regular time intervals, by interpolating the electron density at appropriate time delays at the four different spatial positions. We have done this in Fig. 4(b) for three assumptions about the expansion velocity, spanning the expected values from experiment[10] and simulation[32] under the same conditions. It is clear from the results that the electron density does indeed fall faster than expected for a simple 3D expansion.

Three major recombining mechanisms can be considered: radiative recombination (RR), dielectronic recombination (DR), and three-body recombination (3BR). RR and 3BR rates were calculated using the semiempirical formulas used by earlier workers.[33] For RR,[34] an electron density of 10^{17} cm s^{-1} and a temperature of 1.5 eV would give a recombination time for singly ionized Mg of $\sim$30 μs with longer time scales as the density and temperature fall later in the expansion. For 3BR,[34] under the same conditions, the recombination times are $\sim$8 μs to the ground state and $\sim$3 μs to the first excited state. Less bound levels recombine
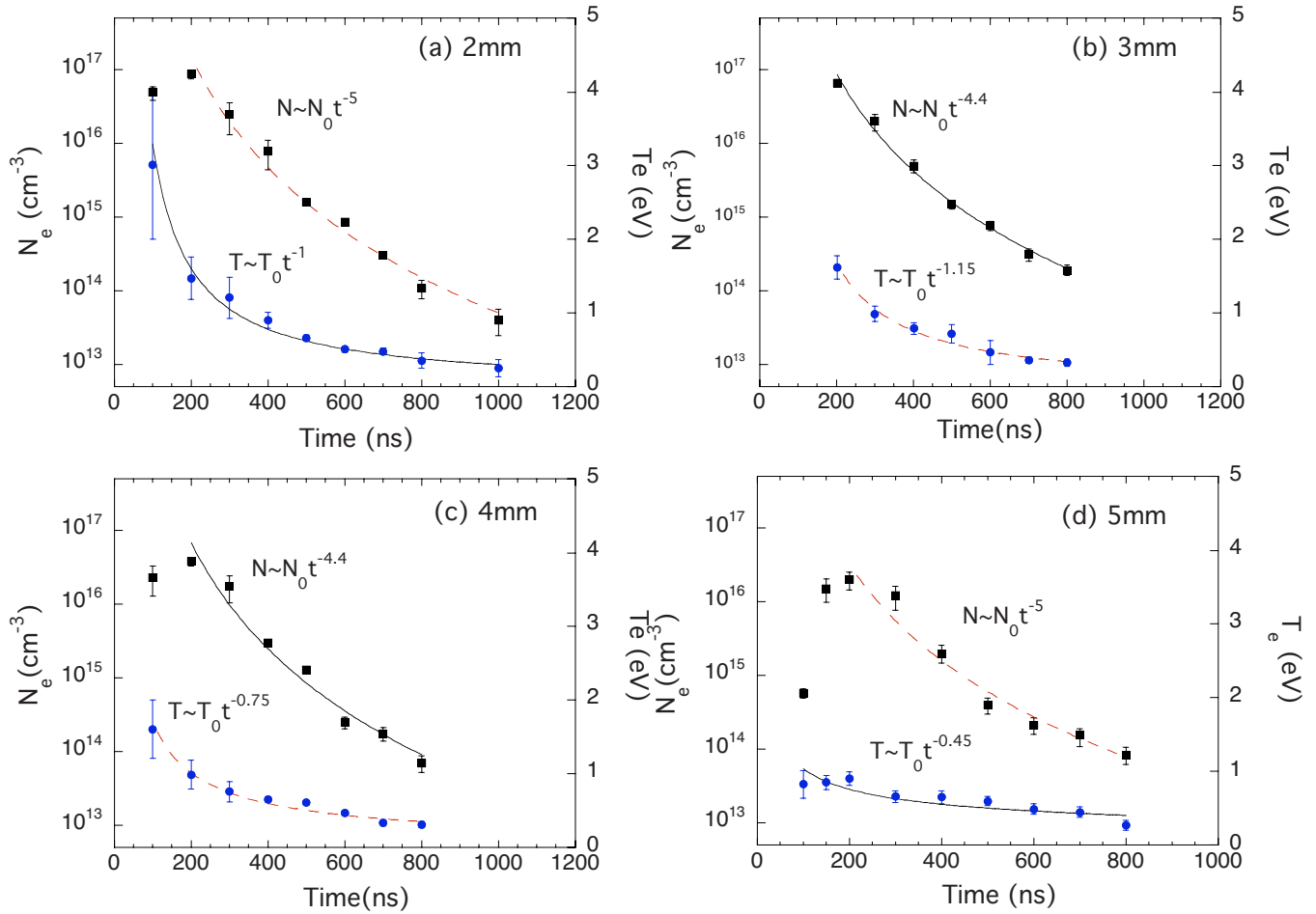
FIG. 3. (Color online) Evolution of the electron density and temperature with time delay, for the plasma probed at (a) 2 mm, (b) 3 mm, (c) 4 mm, and (d) 5 mm from the target.

more readily with this mechanism, but higher levels close to the ionization edge can also be collisionally ionized again very easily. With density falling rapidly this mechanism, with its strong density scaling, cannot account for the drop in ionization.

As pointed out by Thum-Jaeger *et al.*[33] reliable experimental values of the DR rates coefficient can be difficult to obtain. However, experimental measurement of the DR cross section, made by crossing beams of electrons and singly ionized magnesium, Mg^+ (Refs. 35 and 36) suggests a cross
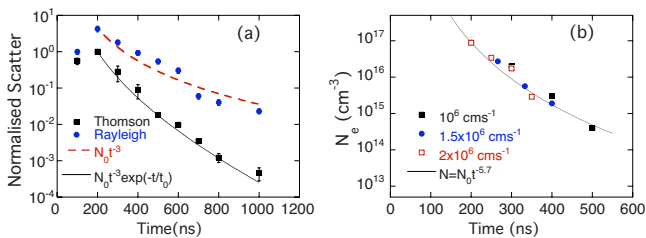

FIG. 4. (Color online) (a) Evolution of normalized electron density (filled squares) compared to normalized Rayleigh scattering intensity (filled circles), which is proportional to the number density of atoms in the plasma plume 2 mm from the target surface. The dashed line is a fit to $N \propto t^{-3}$; the solid line is a fit to $N_e \propto \exp(-t/t_0)t^{-3}$, where $t_0 = 230$ ns. (b) Plot of interpolated electron densities taken at each of the four spatial positions assuming three different expansion velocities (note that all three cases share the data point at 200 ns). The solid line is a fit to $N_e \propto t^{-5.7}$.

section that is consistent with recent calculations of Altun *et al.*[37] Using the fits of Altun *et al.* we obtain a DR rate of 4×10^{-11} $cm^3 s^{-1}$ for $T = 1.5$ eV. This means that at $N_e = 10^{17}$ cm^{-3}, we should have a typical recombination time of order 250 ns. Of course the recombination rate falls with density and thus the time scale lengthens during the expansion, but we can see that at least initially, it is consistent with the empirically derived time scale from the data in that, unlike RR and 3BR, the range of time scales is short enough to allow recombination to be accounted for in the data. We should inject a note of caution and remember that the DR rates are subject to density effects that reduce the recombination rate by removing bound states close to the ionization limit, but are also subject to electric field effects that can enhance the rate. The complex environment of the ablated plasma is not a good testbed to make confident assertions about the DR rate. Nevertheless, our point here is that, from the experimental evidence, recombination is occurring on a time scale of a few hundreds of nanoseconds and DR seems to provide a feasible mechanism, while the other rates considered seem to be too slow.

Turning to the electron temperature, this is found to decay with a dependence close to $T_e \propto t^{-1}$ at 2 mm from the target moving to a slower decay further out. This is in agreement with previous experiments and analytical calculation.[38]
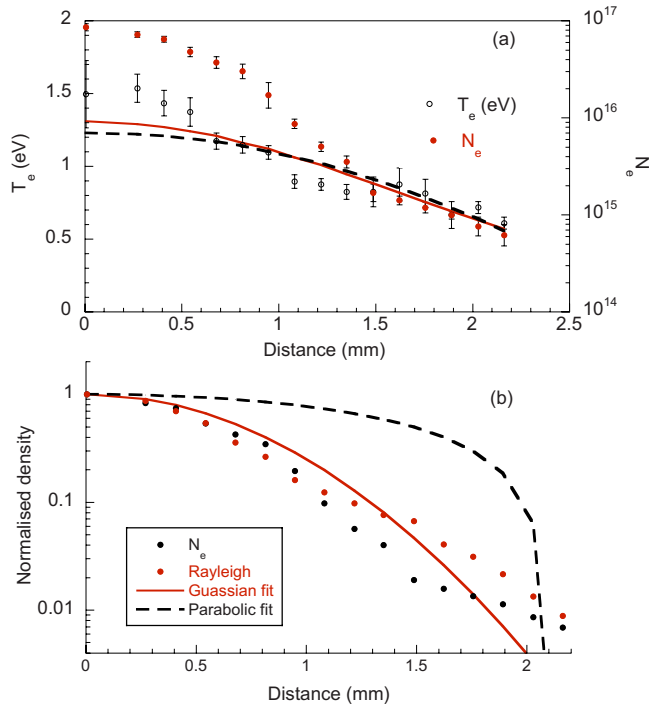
FIG. 5. (Color online) (a) Lateral profile of the electron density and temperature at 2 mm from the target surface and 200 ns after heating. The solid and dashed lines correspond to Gaussian and parabolic fits to the temperature profile. (b) Electron density normalized to the Rayleigh scatter with both Gaussian (solid line) and parabolic (dashed line) fits to the Rayleigh profile.
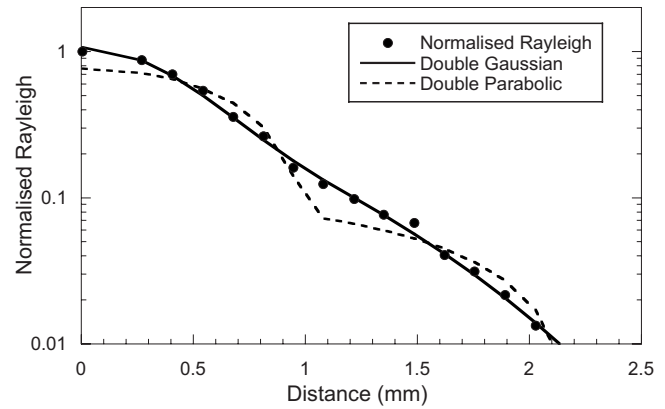

FIG. 6. Normalized lateral profile of the Rayleigh scatter at 2 mm from the target surface and 200 ns after heating. The solid and dashed lines correspond to double Gaussian and double parabolic fits.

This cooling rate is slower than the $T_e \propto t^{-2}$ decay expected with a simple adiabatic expansion and may be explained by transfer of energy to electrons by 3BR which is expected to become important at a time when the free electron thermal energy has fallen to much less than the ionization energy, I_p. According to Rumbsy *et al.*[38] in this situation a very small 3BR rate can lead to sufficient energy transfer to the electrons to make a large change in the electron temperature decay rate without necessarily affecting the density decay rate. For example, the ~ 8 μs decay time mentioned above is slow compared to the $\lesssim 1$ μs evolution of the plume observed and does not account for the ionization drop, but each recombination corresponds typically to ~ 10 eV (i.e., $I_p + 1.5 k T_e$) and a rate of energy transferred to the free electrons of around 1.3 eV/μs per electron.

B. Comparison with plume expansion models

We can compare the density data to simple plume expansion models[31] assuming either isentropic or isothermal expansions. In the former, it is usual to expect a Gaussian spatial profile of density, and in the latter a parabolic spatial and temperature profile. In Fig. 5, we can see the electron density spatially resolved across the plume in the direction parallel to the target surface. A comparison of spatial width of the Rayleigh signal from different times indicated that the average radial expansion velocity of the plume was $4.7 \pm 0.6 \times 10^5$ cm s^{-1}. We can see in Fig. 5 that the ionization is lower in the outer part of the plume and that the electron temperature drops as we move to the outer part of the plume. A fit to the temperature profile can be made with either a

Gaussian or parabolic form. We see that both cases yield more or less equally good fits, the parabolic case being what is expected from an isentropic expansion, while an isothermal expansion should have no gradient. Turning to density, in the lower part of the figure, we can see that a Gaussian fit to the profile, while not perfect, is in better agreement with the general shape than the parabolic profile—the larger range of the density parameter compared to temperature helps to highlight the difference between the curve fits. This implies that, while there is a temperature gradient, it is shallow enough for the isothermal solution to fit best to density. It is worth noting that for the ~ 1 eV temperatures seen in Fig. 5 the electron thermal velocity exceeds the expansion speed thus allowing efficient thermal diffusion across the plasma.

In Fig. 6, we can see the effect of fitting to a double Gaussian and a double parabolic profile, i.e., two profiles with different scale lengths and amplitudes. As we can see, the double Gaussian case gives a better fit than the parabolic and fits better than a single Gaussian profile. Analysis of the best fit parameters suggests two populations of atoms, a smaller one with a lateral velocity of $\sim 10^6$ cm s^{-1}, similar to the axial velocity fits and one with a lateral velocity of $\sim 2.6 \times 10^5$ cm s^{-1}, substantially less than the average lateral velocity inferred from the single Gaussian fit. Multicomponent plumes have been observed in the past, for example, using LIF.[30] One possible interpretation is that the faster plume comes from a plasma created and heated during the beam interaction and that the slower moving component is a result of evaporation from the melt pool on the surface of the solid target. In the axial direction, we only have four positions so we cannot sensibly attempt to fit a double Gaussian spatial profile; a slow component may not even reach the first spatial position at 2 mm until late in time. The axial velocity of expansion is expected to be greater than the lateral expansion, but the aspect ratio should depend on factors such as the focal spot size. For a plume coming from the melt pool and one from the plasma above the surface, we do not necessarily expect the same aspect ratio. Better spatial resolution along the axial direction may be a key parameter in future experiments.

Apart from the density and atomic mass of the target, the input parameters to the models discussed in Ref. 31 include
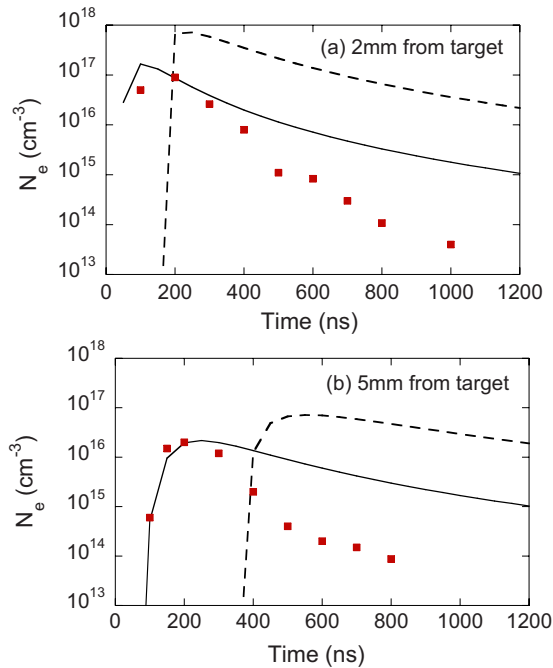
FIG. 7. (Color online) Comparison of experimental and simulated electron density at (a) 2 mm and (b) 5 mm from the target surface. The isothermal solution is the solid line and the isentropic model is represented by the dashed line. The models assume a fixed ionization degree of 1.7 and an ablated vapor mass of 0.12 μg.

the dimensions of the focal spot (in this case 1×1 mm^2) and the depth of the initial melt layer that provides the plume vapor. The estimation of this depth is an important parameter. Using a simple model presented in Ref. 39, we use the thermal conductivity, melting point (903 K), latent heat of vaporization and reflectivity (0.84) of the Mg target to estimate a threshold fluence for ablation of 1.3 J cm^{-2}. Using this, we go on to estimate a melt depth of 1.3 μm per pulse. This gives a vapor mass of 2.3 μg for a 1×1 mm^2 focal spot. A detailed computer simulation, using a two-dimensional hydrocode,[32] indicated a vapor mass of ~ 2 μg with an axial expansion speed of 1.2×10^6 cm s^{-1}. This latter number is in broad agreement with experimental[13] expansion velocities of 1.7×10^6 cm s^{-1}.

In Fig. 7, we can see the comparison of the expansion models with the data. Because the Rayleigh signal for the metastable Mg I state is two orders of magnitude greater than for the ground state of either the neutral or ionized species,[29] we cannot reliably use this as a density diagnostic since it is very sensitive to even a small metastable population. Instead, we have assumed that at the highest density conditions at 2 mm distance ($\sim 10^{17}$ cm^{-3}), we have local thermodynamic equilibrium (LTE) at 1.5 eV; thus we obtain an average ionization of 1.7 and use this to estimate atomic densities from the electron density. Using this, we can match the predicted density for the isothermal expansion case early in time, but only by assuming substantial absorption in the vapor plume that reduces the effective fluence on the solid surface to ~ 1.7 J cm^{-2}. For the isentropic expansion, we would need to assume an even smaller effective absorption at the solid surface and in general we can see that we do not get a good match in the time at which peak density is reached at a given

distance from the target. At both distances, we can see that the predicted density, which is based on a fixed ionization degree, falls more slowly than the experimental value. This is consistent with recombination of the electrons as discussed above. We note that in Ref. 39 the ablated depth per pulse for Cu targets using this model was compared with experimental data[40] using a similar KrF laser at similar fluences up to 8 J cm^{-2}. In that case, a good match was found when the absorption was reduced from the standard reference value of 0.6–0.03 to account for the shielding effect of the plasma vapor generated.

The predicted vapor mass is now only 0.12 μg, substantially lower than seen in the simulation in Ref. 32. One candidate for absorption is inverse bremsstrahlung. A detailed treatment would need to account for the ignition of the plasma and the propagation of the beam all the way to the critical density surface, which for a KrF laser is at $\sim 1.6 \times 10^{22}$ cm^{-3}. One possibility to consider is the early ignition of the plasma. In the modeling,[32] the laser beam has an average irradiance that varies smoothly across the beam. In the experiment, however, we used random phase plates to give a beam that is smooth on long spatial scales. The mechanism for the operation of phase plates is that they break the beam up into many beamlets with a phase difference between beamlets of π or 0 introduced randomly. This means that, at the focal plane, we have overlapping interfering beams with sharp fixed intensity "spikes" on a small spatial scale. In theory these are so closely spaced that thermal conduction is then very effective in smoothing the pressure at the ablation front. It is possible that such spikes in intensity will also ignite a vapor plume into a plasma very easily and earlier in the pulse than would be seen for a truly smooth profile. If ignition occurs early in the pulse, then there might be significant absorption away from the solid density surface, thus explaining the low ablated vapor mass. The inverse bremsstrahlung absorption coefficient is given by

$$\alpha_{\mathrm{IB}} = 3.7 \times 10^8 \frac{Z(N_e)^2}{\nu^3 T^{1/2}} (1 - \exp(-h\nu/kT)) \text{ cm}^{-1}, \qquad (1)$$

where T is in K and the electron density is in cm^{-3}. We can see that at 100 times less than critical density and 2 eV with $Z=2$, the absorption coefficient is still only ~ 65 cm^{-1} giving an absorption depth of 150 μm. If we assume that a typical scale length of the plasma is given by $L \sim V_{\mathrm{ex}} t_p$, i.e., the expansion velocity multiplied by the rise time to the peak of the pulse (about 5 ns in this case) then we get a scale length of only ~ 60 μm. This shortens close to critical density, but then the higher densities are closer to and thermally more strongly coupled to the solid bulk, thus reducing the effect of absorption at critical density on ablated mass.

A possibly more important role may be played by photoionization of metastables by laser light in the plume. During the pulse, in the high density vapor close to the target, we would expect the metastable $^3P^0$ term in Mg I to be heavily populated. This level has an ionization potential of 4.9 eV, just below the 5.0 eV photon energy of the KrF beam. Evidence of these metastable states is seen in the data displayed above. The cross section for photoionization from this meta-
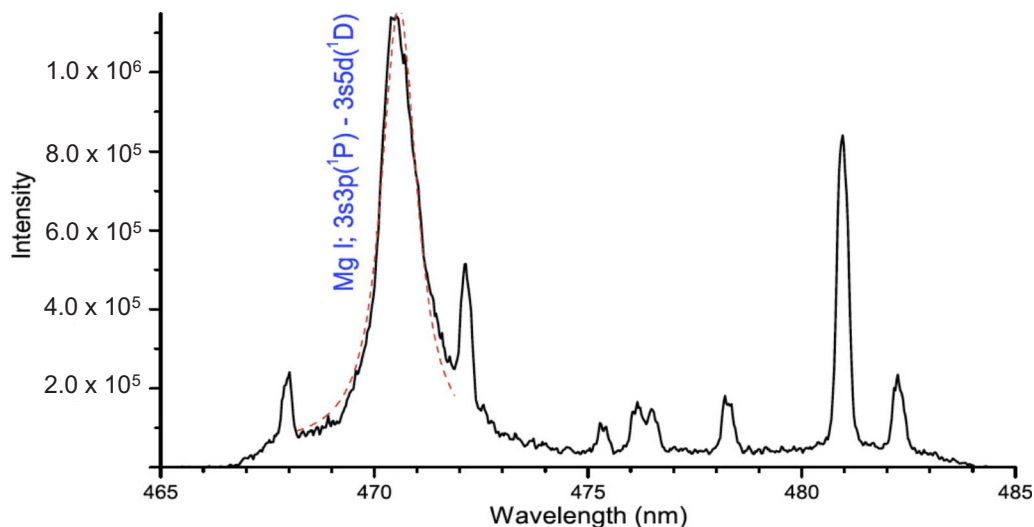
FIG. 8. (Color online) High resolution emission spectrum from a Mg plume, 100 ns delay 2 mm from the target surface. The gate time for the ICCD was 10 ns for all the emission spectra. The spectrum is an accumulation of 25 shots. The peak at 470.3 nm is fitted with a Voigt function.

stable level[41] is 1.4×10^{-17} cm^2. This means that for a metastable density of 100 times less than critical, the absorption length is only ~ 5 μm and we can see that strong absorption is indeed possible. The cross section per atom for photoionization in the initial plume is independent of the plume density and this may contribute to a more uniformly heated initial vapor mass and thus a more uniform temperature in the plume; this helps explain the relative success of the isothermal model in fitting the data compared to the isentropic model. An interesting possibility is in future to compare the results here to data for Mg ablation with a fourth harmonic Nd:YAG laser at 266 nm, with a photon energy just below the photoionization limit of the Mg metastables. This would confirm or refute the importance of photoionization.

IV. COMPARISON WITH EMISSION SPECTROSCOPY RESULTS

It is interesting to compare the results of Thomson scatter with those of emission spectroscopy. Using the same experimental arrangement, we recorded emission spectra for the Mg plume in the 465–480 nm regime. With the imaging system, we retained the spatial resolution in the lateral expansion direction and, in the axial expansion direction, since we make an image of the plume onto the spectrometer slit, we effectively select a narrow region from which emission is recorded. However, the volume sampled is less defined than for the Thomson scatter since we look along a line of sight through the plume. In Fig. 8 we see the strong $3s3p$ ^1P-$3s5d$ ^1D emission line at 470 nm.

It is expected that under the experimental conditions here, the principal broadening mechanism is electron impact Stark broadening and we have used this to infer the electron density as a function of time and distance along the plume. We can see in Fig. 8 that the FWHM of the line is greater than 1 nm. By contrast, the contribution from Doppler broadening is estimated at 0.04–0.13 nm using the range of electron temperatures from the Thomson scatter (which is likely to overestimate the ion temperature). In Fig. 9, we can see the temporal history at 2 mm from the target surface. The

error bars mainly reflect different choices of T_e, either from the emission spectroscopy (see below) or Thomson scatter.

We can see that Fig. 9 shows a slower fall in electron density with time from Stark widths than the equivalent Thomson scatter data. This may be due to several reasons: uncertainty in the Stark parameters, averaging through a line of sight through the plume, or higher ion temperature and thus Doppler width than expected. At lower density, the latter becomes a more important contribution to the width. For determination of the temperature from spectral emission, we have studied a wider spectrum using the same collection optics but feeding the signal into a smaller 1/8 m spectrometer with lower dispersion fitted with a 400 line/mm grating blazed at 400 nm. The system was calibrated with a Zn/Hg/Cd lamp. The BK7 exit window limited the lower spectral cutoff to 370 nm. Nevertheless, we recorded spectra, as seen in Fig. 10, with seven Mg I lines identified. Other smaller features were unidentified but could come from the
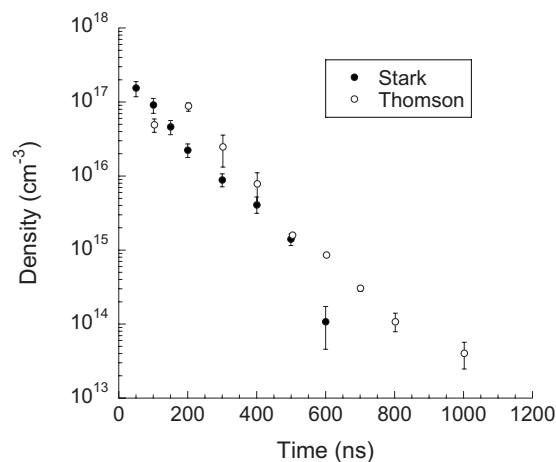

FIG. 9. Electron density evolution with time for plasma 2 mm from the target surface, determined by calculating the Stark width of the emission line of Mg I at 470.3 nm, compared to results from Thomson scatter. The agreement is not perfect with an apparently slower fall with time for the Stark data.

(a) $d = 2mm$; $\Delta t = 200ns$
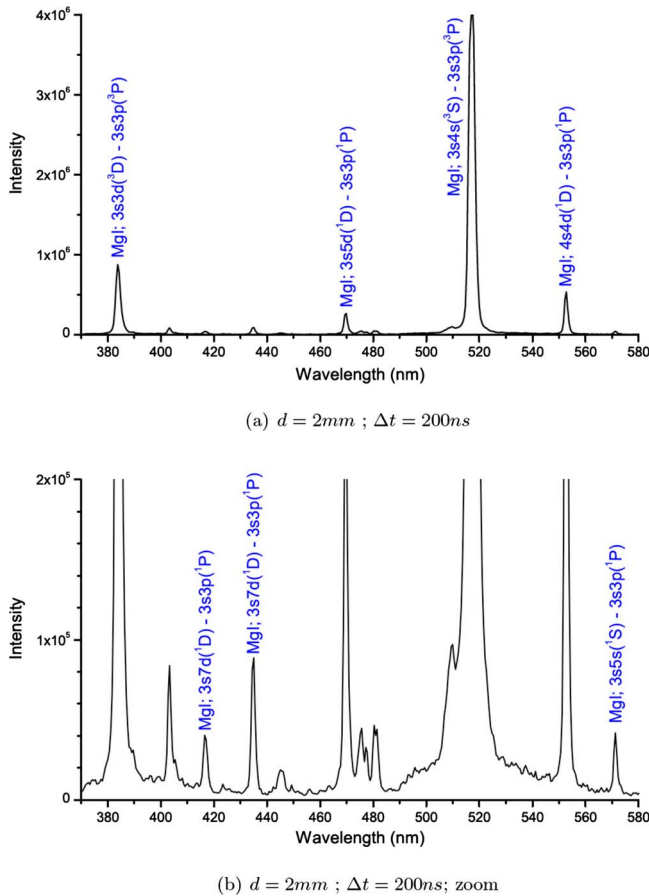

(b) $d = 2mm$; $\Delta t = 200ns$; zoom

FIG. 10. (Color online) Emission spectrum recorded with lower dispersion spectrometer (a) principal lines and (b) zoomed spectrum to show weaker lines.

1% impurity content. The advantage of the lines used is that they all have an excited state as the lower level, thus reducing the potential impact of opacity.

In order to determine temperature, we have made use of a Boltzmann plot for the different lines, as seen in Fig. 11, where we can see the resulting plots for two different time delays, again at 2 mm from the target surface. The data do not lie on a perfect straight line as expected for LTE. This may be a result of opacity effects, which would be strongest for the $3s3p$ ^3D-$3s3p$ ^3P line at 383.2 nm. This line has an
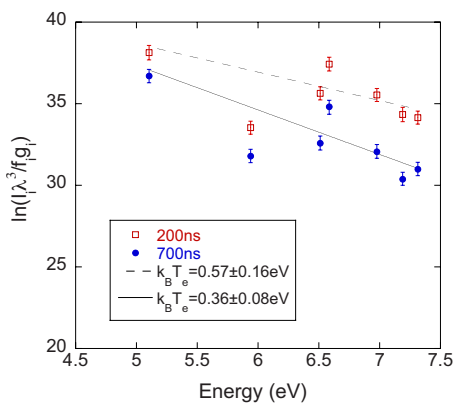

FIG. 11. (Color online) Boltzmann plots of line ratios for Mg emission at 2 mm from target for (a) 200 ns delay and (b) 700 ns delay.

oscillator strength (0.499) that is approximately four times greater than any of the other lines and, for that reason, we have fitted the straight lines ignoring this transition (seen on the plot with upper state 5.95 eV). We see that early in time we get a temperature of 0.57 ± 0.16 eV, which is lower than the 1.5 eV seen from the Thomson scatter. At later time (700 ns) the optical emission gives us 0.36 ± 0.08 eV compared to 0.5 eV from the Thomson scatter. This better agreement at later time may be a result of smaller opacity effects but also may be due to the effect of sampling a line of sight through the plume: we can see in Fig. 5 that the temperature in the outer part of the plume drops to ~ 0.5 eV; thus averaging may lower the spectral temperature seen. At later time we expect the temperature to be more isothermal. We can also note that, in both cases, we have assumed partial local thermodynamic equilibrium (PLTE); in other words, the collisional rates are assumed to dominate over radiative rates in setting the population levels. An earlier paper using a collisional radiative model of Mg (Ref. 42) suggests that in a Mg plume, under similar conditions, the spectral line ratios from Mg I may underestimate the actual temperature if PLTE is assumed and that also, time dependent effects are likely to be important in the spectrum formation.

V. CONCLUSIONS

To conclude, we have used Thomson scattering to make direct and fairly unambiguous measurements of the electron temperature and density in a Mg laser produced plasma. The rapid drop in electron density seems to be explained by DR with recent calculations in broad agreement with the time scale seen experimentally. The measured electron temperature varied with a t^{-1} time dependence; this result is consistent with an expansion of the plasma where 3BR injects energy into electrons, reducing the rate at which the electrons are cooling. Comparison of the experimental electron density evolution in the axial direction and the spatial profile laterally, with simple expansion models, indicates that an isothermal approximation better fits the data than an isentropic expansion. The comparison with the models also indicates a significantly reduced ablated vapor mass, presumably due to significant absorption. The best candidate for the dominant absorption mechanism is photoionization from the metastable state of Mg I. The emission spectroscopy of the plume yields electron density and temperature data that, while broadly consistent with the Thomson scatter data, show some differences that may be due to line-of-sight averaging, opacity, and time dependence of ionization. The comparison is useful in highlighting problematic issues in emission spectroscopy such as volume sampling and opacity. There is evidence from the lateral expansion data that there is a faster plume component, smaller in density than the main plume, that comes from the laser heated plasma above the target surface.

[1] K. L. Saenger, Process. Adv. Mater. **39**, 63 (1993).

[2] H. F. Sakeek, M. Higgins, W. Graham, T. Morrow, R. Turner, and D. Walmsley, J. Appl. Phys. **70**, 2455 (1991).

[3] P. E. Dyer, A. Issa, and P. Key, Appl. Phys. Lett. **53**, 534 (1988).

[4] J. Ihlemann, A. Scholl, H. Schmidt, and B. Wolff-Rottke, Appl. Phys. A: Mater. Sci. Process. **60**, 411 (1995).

[5] K. H. Song and X. Xu, Appl. Phys. A: Mater. Sci. Process. **65**, 477 (1997).

[6] R. Kelly, Nucl. Instrum. Methods Phys. Res. B **46**, 441 (1990).

[7] D. B. Chrisey and G. K. Hubler, *Pulsed Laser Deposition of Thin Films* (Wiley, New York, 2003).

[8] S. Pramanick, A. Kumar, and J. Narayan, Jpn. J. Appl. Phys., Part 1 **32**, 789 (1993).

[9] I. Weaver, G. Martin, W. Graham, T. Morrow, and C. Lewis, Rev. Sci. Instrum. **70**, 1801 (1999).

[10] L. Doyle, G. Martin, W. Graham, T. Williamson, A. Al-Khateeb, I. Weaver, D. Riley, M. Lamb, and T. Morrow, IEEE Trans. Plasma Sci. **27**, 128 (1999).

[11] G. Martin, T. Williamson, L. Doyle, A. Al-Khateeb, I. Weaver, D. Riley, M. Lamb, T. Morrow, and C. L. S. Lewis, IEEE Trans. Plasma Sci. **27**, 130 (1999).

[12] I. Weaver, L. Doyle, G. Martin, D. Riley, M. Lamb, W. Graham, T. Morrow, and C. Lewis, Proc. SPIE **3404**, 341 (1998).

[13] L. Doyle, G. Martin, A. Al-Khateeb, I. Weaver, D. Riley, M. Lamb, T. Morrow, and C. Lewis, Appl. Surf. Sci. **127–129**, 716 (1998).

[14] A. Delserieys, F. Y. Khattak, C. L. S. Lewis, and D. Riley, Appl. Phys. Lett. **92**, 011502 (2008).

[15] J. Sheffield, *Plasma Scattering of Electromagnetic Radiation* (Academic, London, 1975).

[16] T. P. Hughes, *Plasma and Laser Light* (Adam Hilger, London, 1975).

[17] D. E. Evans and P. G. Carolan, Phys. Rev. Lett. **25**, 1605 (1970).

[18] A. A. Offenberger and R. D. Kerr, Phys. Lett. A **37**, 435 (1971).

[19] R. Behn, Appl. Phys. Lett. **36**, 363 (1980).

[20] H. Rohr, K. H. Steuer, G. Schramm, K. Hirsch, and H. Salzman, Nucl. Fusion **22**, 1099 (1982).

[21] S. H. Glenzer, Phys. Plasmas **6**, 2117 (1999).

[22] M. D. Bowden, Y. Goto, H. Yanaga, P. J. A. Howarth, K. Uchino, and K. Muraoka, Plasma Sources Sci. Technol. **8**, 203 (1999).

[23] S. A. Moshkaylov, C. Thompson, T. Morrow, and W. G. Graham, J. Vac. Sci. Technol. A **18**, 1395 (2000).

[24] G. Gregori, U. Kortshagen, J. Heberlein, and E. Pfender, Phys. Rev. E **65**, 046411 (2002).

[25] T. V. George, A. G. Englehar, and C. DeMichelis, Appl. Phys. Lett. **16**, 248 (1970).

[26] C. L. S. Lewis, I. Weaver, L. Doyle, G. Martin, T. Morrow, D. A. Pepler, C. N. Danson, and I. N. Ross, Rev. Sci. Instrum. **70**, 2116 (1999).

[27] M. Sneep and W. Ubachs, J. Quant. Spectrosc. Radiat. Transf. **92**, 293 (2005).

[28] NIST Atomic Spectra Database (version 3.1.2), URL: http://physics.nist.gov/PhysRefData/ASD/levels_form.html.

[29] A. Delserieys, F. Y. Khattak, S. Sahoo, G. Gribakin, C. L. S. Lewis, and D. Riley, Phys. Rev. A **78**, 055404 (2008).

[30] G. Martin, L. Doyle, A. Al Khateeb, I. Weaver, D. Riley, M. Lamb, T. Morrow, and C. Lewis, Appl. Surf. Sci. **127–129**, 710 (1998).

[31] M. W. Stapleton, A. P. McKiernan, and J.-P. Mosnier, J. Appl. Phys. **97**, 064904 (2005).

[32] M. S. Quaisar and G. J. Pert, J. Appl. Phys. **94**, 1468 (2003).

[33] A. Thum-Jaeger *et al.*, Phys. Rev. E **61**, 3063 (2000).

[34] A. C. Kolb and R. W. P. McWhirter, Phys. Fluids **7**, 519 (1964).

[35] D. S. Belic, Phys. Rev. Lett. **50**, 339 (1983).

[36] K. J. LaGattuta and Y. Hahn, J. Phys. B **15**, 2101 (1982).

[37] Z. Altun, A. Yumak, N. R. Badnell, S. D. Loch, and M. S. Pindzola, Astron. Astrophys. **447**, 1165 (2006).

[38] P. T. Rumsby and J. W. M. Paul, Plasma Phys. **16**, 247 (1974).

[39] S. Amoruso, R. Bruzzese, R. Velotta, and N. Spinelli, J. Phys. B **32**, R131 (1999).

[40] J. G. Lunney, Appl. Surf. Sci. **86**, 79 (1995).

[41] T. N. Rescigno, Phys. Rev. A **31**, 607 (1985).

[42] D. Riley, I. Weaver, T. Morrow, M. J. Lamb, G. W. Martin, L. A. Doyle, A. Al-Khateeb, and C. L. S. Lewis, Plasma Sources Sci. Technol. **9**, 270 (2000).